Origin of electric-field gradients in high-temperature superconductors: $YBa_2Cu_3O_7$

Jaejun Yu and A. J. Freeman
Department of Physics and Astronomy, Northwestern University, Evanston, Illinois 60208

R. Podloucky and P. Herzig
Institute for Physical Chemistry, University of Vienna, A-1090 Vienna, Austria

P. Weinberger
Institute for Technical Electrochemistry, Technical University of Vienna, A-1060 Vienna, Austria
(Received 5 February 1990; revised manuscript received 27 July 1990)

The origin of the electric-field gradients (EFG) at nuclear sites in the high-T_c superconductor $YBa_2Cu_3O_7$ is investigated theoretically by means of highly precise local-density full-potential linearized-augmented-plane-wave calculations. In all cases considered (i.e., at Cu, O, Ba, and Y nuclei), the theoretical predictions for the principal axis V_{zz} and the anisotropy parameter η of the EFG tensor agree well with available experiments and the results of Ambrosch-Draxl *et al.* The principal axis at O sites are found to lie in the direction of the Cu-O $dp\sigma$ bonding axis, and the oxygen η values are largely determined by the internal anisotropy inside the oxygen spheres. This is consistent with the finding that the main contribution to the EFG at the Cu sites comes from the intrinsic quadrupole field provided by the nonspherical (internal) charge distributions surrounding each Cu atom arising from the strong anisotropic hybridization between Cu d and O p electrons. Surprisingly, the (Sternheimer antishielding) contribution from the core electrons—mainly from the Cu $3p$ "semicore" electrons—is found to be very small. Overall, the agreement of the oxygen EFG components themselves with experiment is good. The calculated V_{zz} values are within 20% of the experiment, except for Cu(2), which is only half of the observed value and results in a reversal of the relative magnitude of the EFG at Cu(1) and Cu(2) sites. This error may result from the inexact treatment of the $3p$ semicore states when they are allowed to relax and are described as band states. This is seen from the extreme sensitivity of the EFG to the calculated anisotropic charge distributions of the core electrons. Thus, a transfer of only 0.0014 electrons from Cu(2) $3p_x$ and $3p_y$ to $3p_z$ would enhance the EFG value and produce perfect agreement with experiment.

I. INTRODUCTION

Both experiment and theory have emphasized one of the most interesting characteristics of the high-T_c superconductor $YBa_2Cu_3O_7$ to be the major role played by the CuO_2 planes and CuO chains for the superconducting state. Our early electronic structure calculations[1,2] showed the distinct two-dimensional and one-dimensional features of the electronic structure arising from the CuO_2 planes and CuO chains, respectively, and a possible interplay between the electrons in the planes and chains was suggested. Recent nuclear magnetic resonance (NMR) and nuclear quadrupole resonance (NQR) experimental studies of $YBa_2Cu_3O_7$ have provided important insights into the microscopic properties of this superconductor. Two NQR resonance lines were observed at 22 and 31.5 MHz, which appear to match the two distinct (plane and chain) Cu sites in $YBa_2Cu_3O_7$. Warren *et al.*[3] found strikingly different relaxation behavior for these two resonance lines in the superconducting state, implying the existence of two very different superconducting energy-gap structures for the plane and chain Cu sites. At that time, some groups,[3,4] in disagreement with other experimental work,[5] assigned the 31.5-MHz resonance to arise from the chain Cu(1) site and the 22-MHz resonance from the Cu(2) plane site. This assignment was later reversed: while yielding similar relaxation behavior, recent NMR and NQR studies of single crystals, oriented powders, and relaxation measurements on $(R)Ba_2Cu_3O_7$ lead to the convincing assignment that the 22-MHz resonance arises from the Cu(1) chain site and the 31.5-MHz resonance arises from the Cu(2) plane site.[6]

In view of the importance of the relaxation measurements and site assignments we have attempted to provide theoretical information on the electric field gradients at each Cu site in $YBa_2Cu_3O_7$. As the NQR spectra arise from the nuclear (electronic) quadrupole interaction which is determined by the distribution of the electronic charge surrounding the nuclei, the NQR resonance lines reflect the static electronic structure near each nuclear site embodied in the electric field gradient (EFG). In this paper[7] we calculate the EFG's by means of the self-consistent full-potential linearized augmented-plane-wave method (FLAPW)[8] which makes no shape approximation to the electronic potential and, furthermore, takes all electrons, core as well as valence states, into account for the construction of the potential. From the angular dependence of the potential at the nuclear sites, the EFG for the corresponding nuclei is directly derived (cf. Sec. II). As shown by Refs. 9 and 10, a FLAPW based ap-

proach is able to yield reliable results for the EFG, at least for bulk systems with high-symmetry local environments, which, however, is not the case for $YBa_2Cu_3O_7$. For this compound we face the difficulty that the orthorhombic unit cell contains 8 nonequivalent atomic positions. Hence, to obtain convergence and the necessary precision for such a system by the FLAPW approach, one has to perform demanding numerical calculations. Fortunately, this can be done today treating all the electrons—core and conduction—thanks to the power of modern computers. The results obtained are very close to those obtained by Ambrosch-Draxl *et al.*[11] using the FLAPW method. Thus these results serve to confirm the validity and consistency nowadays of highly precise electronic structure calculations.

As a point of departure, consider the origin of the EFG at nuclei in solids which has been studied for many years, following the work of Steinheimer,[12] employing either asymmetric internal charge distributions in nonoverlapping atoms or ions or quadrupolar external crystalline fields (arising from a lattice of point charge) on a closed shell atom or ion.[13] In both cases, the quadrupole polarization of the closed shells of the core electrons is found to play an important role (so-called Steinheimer antishielding). Thus, in this simple approach, there are basically two contributions to the EFG at a nuclear site. One, $q_{\rm int}$, is from internal charge distributions and the other, $q_{\rm ext}$, from external charge distributions. If one includes their respective Sternheimer antishielding factors, the total EFG (i.e., V_{zz}) is usually written as

$$q = q_{\rm int}(1-R) + q_{\rm ext}(1-\gamma_\infty) , \tag{1}$$

where R is an internal shielding factor (usually less than one) and γ_∞ is an external antishielding factor ($|\gamma_\infty|$ can be as large as 20 for $3d$ ions).

In a real many-electron many-(overlapping) atom systems like $YBa_2Cu_3O_7$, the physics is of course more complicated. While the calculation of the EFG arising from aspherical valence electrons is straightforward in an FLAPW band calculation, one also needs to determine the role of the core electrons (Steinheimer antishielding) on the EFG. This proves to be a somewhat difficult task in that a proper description of anisotropic core electron charge distributions is not easily achievable within the FLAPW approach.

It turns out that much of the theoretical-computational work in this paper is addressed to this problem. Early on,[7] we carried out standard FLAPW calculations in which the Cu $3p$ electrons were treated as (spherical shell) core electrons. We found overall agreement of our calculated EFG values with experiment—except for a reversal in the relative ordering [Cu(1) vs Cu(2)] between theory and experiment. In order to calculate the contribution of the core electrons—particularly the Cu $3p$ "semicore" electrons—we relaxed the spherical restraint by treating the $3p$ levels as band states. We find that the main contribution to the EFG at Cu sites in $YBa_2Cu_3O_7$ is not the external field but the "intrinsic" quadrupole field provided by the nonspherical (internal) charge distribution inside each Cu atom. These large nonspherical charge distributions are mostly due to strong anisotropic hybridization between Cu d and O p states in $YBa_2Cu_3O_7$. The contribution from the core electrons (Steinheimer antishielding) is found to be surprisingly small. Nevertheless, a transfer of only 0.0014 electrons from the (so-called "semicore") Cu $3p_x$ and $3p_y$ states to the $3p_z$ state would easily enhance the (otherwise low) value of the EFG at Cu(2) and so would reproduce the experimental result.

In Sec. II, equations for the EFG are given together with some details about the FLAPW calculations. In Sec. III, the calculated EFG values at the Cu sites as well as at the other site (i.e., O, Ba, and Y) are given and compared with experiment. An analysis of the charge density decomposition and its contribution to the EFG is made in order to study the origin of the EFG at the Cu sites in $YBa_2Cu_3O_7$. It is found that the main contribution to the EFG at the Cu sites comes from the intrinsic quadrupole (internal) charge distributions inside the Cu atoms. Later in Sec. IV, a detailed analysis is presented of the charge anisotropy and its relation to the EFG. It is also shown that the anisotropy of the charge distribution is due to the covalent nature of the Cu d-O p hybridization. From the relation between the charge anisotropy and its contribution to the EFG, the EFG results for Cu(2) are found to be extremely sensitive to the charge anisotropy of the Cu $3p$ semicore electrons. Finally, concluding remarks are made in Sec. V which focuses on the importance of a proper treatment of core electrons by energy band methods. In Appendix A, we present details of our "two-window" FLAPW approach which is employed to describe the semicore electrons as band states.[14]

II. CALCULATIONAL DETAILS

A. electric field gradient

The all-electron Coulomb potential $V(r)$ is obtained by solving Poisson's equation for a self-consistent electron charge density $\rho(\mathbf{r})$ and nuclear charge Z_i at $\mathbf{r}_i$:

$$V(\mathbf{r}) = \int \frac{\rho(\mathbf{r}')}{|\mathbf{r}-\mathbf{r}'|} d\mathbf{r}' + \sum_i \frac{Z_i}{|\mathbf{r}-\mathbf{r}_i|} , \tag{2}$$

where the index i runs all over the nuclear positions in the lattice. From the potential $V(r)$, the components of the electric field gradient (EFG) tensor at the nuclear sites are derived[15] from

$$\Phi_{ij} = \left. \frac{\partial^2 V}{\partial x_i \partial x_j} \right|_n , \tag{3}$$

where the x_i denotes the x, y, and z axes for $i=1,2,3$. Since there is no nuclear quadrupole interaction with a spherical potential, the EFG tensor is often defined as a traceless tensor

$$\Phi_{ij} = \left. \frac{\partial^2 V}{\partial x_i \partial x_j} \right|_n - \tfrac{1}{3}\delta_{ij} \nabla^2 V|_n . \tag{4}$$

In the case of $YBa_2Cu_3O_7$ with an orthorhombic lattice, the off-diagonal components Φ_{ij} $(i \neq j)$ are zero due to

symmetry. Then the Cartesian coordinate axes x, y, and z become the principal axes. If we rename the components Φ_{ii} by V_{ii} and order them according to their magnitudes, we obtain a new set of orthogonal x', y', and z' axes, such that

$$|V_{z'z'}| \geq |V_{y'y'}| \geq |V_{x'x'}| \ . \tag{5}$$

From the condition that

$$\nabla^2 V = V_{x'x'} + V_{y'y'} + V_{z'z'} = 0 \ , \tag{6}$$

we specify the principal components of the EFG tensor with the two parameters q, the quadrupole moment, and η, the anisotropy parameter, as defined by

$$eq = V_{z'z'} = \frac{\partial^2 V}{\partial z'^2}, \quad \eta = (V_{x'x'} - V_{y'y'})/V_{z'z'} \ . \tag{7}$$

The range of η is $0 \leq \eta \leq 1$.

B. FLAPW method for EFG calculations

In the FLAPW method, a self-consistent charge density $\rho(\mathbf{r})$ is represented by

$$\rho(\mathbf{r}) = \begin{cases} \sum_{L,M} \rho_{LM}(r) Y_{LM}(\hat{r}) & \text{inside MT spheres,} \\ \sum_{\mathbf{G}} \rho(\mathbf{G}) \exp(i\mathbf{G}\cdot\mathbf{r}) & \text{in the interstitial region.} \end{cases} \tag{8}$$

Using the method by Weinert[16] we solve Possion's equation for the anisotropic charge density and have a full-potential $V(\mathbf{r})$ which is represented by

$$V(\mathbf{r}) = \begin{cases} \sum_{L,M} V_{LM}(r) Y_{LM}(\hat{r}) & \text{inside MT spheres,} \\ \sum_{\mathbf{G}} V(\mathbf{G}) \exp(i\mathbf{G}\cdot\mathbf{r}) & \text{in the interstitial region.} \end{cases} \tag{9}$$

Since the full potential takes an asymptotic expression for $|\mathbf{r}| \rightarrow 0$ such that[9,15]

$$V(\mathbf{r} \rightarrow 0) = \sum_{lm} r^l \Phi_{lm} \left[\frac{4\pi}{2l+1} \right]^{1/2} Y_{lm}(\hat{r}) \tag{10}$$

at each nucleus, the tensor component Φ_{lm} of the EFG (i.e., $l=2$) can be determined by

$$\Phi_{2m} = \lim_{r \rightarrow 0} \left[\frac{5}{4\pi} \right]^{1/2} \frac{V_{2m}(r)}{r^2} \tag{11}$$

at the nucleus. These tensor components Φ_{2m} can be rewritten as Cartesian components of Φ_{ij}; for example, for diagonal components,

$$\begin{aligned} \Phi_{xx} &= \left[\frac{3}{2} \right]^{1/2} \Phi_{22} - \Phi_{20} + \left[\frac{3}{2} \right]^{1/2} \Phi_{2-2} \ , \\ \Phi_{yy} &= - \left[\frac{3}{2} \right]^{1/2} \Phi_{22} - \Phi_{20} - \left[\frac{3}{2} \right]^{1/2} \Phi_{2-2} \ , \\ \Phi_{zz} &= 2\Phi_{20} \ . \end{aligned} \tag{12}$$

The EFG's determined by the FLAPW method have been verified by the multipole lattice sum method[15] for a given self-consistent charge density. Using the multipole lattice sum method, we can make a decomposition of EFG's into contributions arising from the muffin-tin region of a given atom, from other atoms' muffin-tin regions and from the interstitial region. This decomposition will be employed to analyze the results.

C. Band structure calculations

The self-consistent local density band-structure calculations were carried out for the *Pmmm* structure[17] using the FLAPW method with the Hedin-Lundqvist approach for the local density approximation to the exchange-correlation potential. Detailed results for the band structure of $YBa_2Cu_3O_7$ were presented previously.[2] Since the EFG requires the second derivative of the potential, the results obtained are extremely sensitive to its convergence (self-consistency); hence, much more precise convergence is requires for the nonspherical components of the charge density than was previously obtained.[2] Specifically, this means that one has to improve the convergence by a careful consideration of controlled numerical parameters such as number of plane waves, spherical harmonics, and k points—as well as running more iterations to reduce the difference between input and output charge density (which is usually taken for defining the quality of the self-consistency).

In order to check the sensitivity of the EFG calculations to the parameters chosen for the expansion of the wave functions, charge density, and potential, we have tested all possible variations of the parameters so as to assess computational limitations. The angular momentum expansion of the wave function inside the muffin-tin spheres was first limited to $l=8$ and then increased to $l=10$. The convergence of the EFG as a function of the number of basis functions was checked by choosing the basis set for $|\mathbf{k}+\mathbf{G}| \leq 3.5$ a.u., resulting in 850 basis functions, and for $|\mathbf{k}+\mathbf{G}| \leq 3.65$ a.u., which led to 950 augmented-plane waves. For the charge density and potential, the lattice harmonics expansion was done for both $l_{\max}=6$ and $l_{\max}=8$ limits inside the muffin-tin spheres whereas the Fourier representations in the interstitial region required over 8000 reciprocal lattice vectors. For the Brillouin zone integrations, 16 sampling $\mathbf{k}$ points and a Gaussian smearing technique were used during the self-consistent iterations. In addition, 36 sampling $\mathbf{k}$ points were used in order to check convergence; we found that the 16 $\mathbf{k}$ point results were sufficiently close to the 36 $\mathbf{k}$ points results. Finally, the number of iterations was increased until the EFG for the corresponding input and output densities varied only within 0.5% from one iteration to the next.

A variety of model calculations were carried out. First, as described above, a "standard" FLAPW calculation was performed in which the Cu $3p$ electrons (and other closed shell core electrons) are treated as core states—and labeled in what follows as "$3p_{\text{core}}$." This means that their charge density is spherically symmetric and so gives no contribution to the EFG. In a second set

of calculations, the Cu $3p$ electrons were treated as band states in the same window as in the standard calculation and hence allowed to have aspherical charge densities which contribute to the EFG (i.e., Steinheimer antishielding). It turned out that the contribution of these aspherical charge densities to the EFG's are so sensitive to their treatment as band states, that this so-called standard "single-window" calculation (in which a single energy parameter was employed in the linearization of the APW) yielded unphysical results.[14] For this reason we performed a "two-window" calculation which included the Cu $3p$, Y $4s$, and Ba $5s$ states into the second window (i.e., their energies fall in the range covered by the second energy parameter). In this case the calculations are referred to as "Cu $3p_{\rm val}$" and these results are quoted below. Details of the two-window method of calculation are described in Appendix A.

III. RESULTS

A. FLAPW results for the EFG at the Cu sites

The theoretical and experimental EFG values at the two distinct Cu-sites in $YBa_2Cu_3O_7$ are listed in Table I. The first line of Table I, referred to as "Cu $3p_{\rm core}$," shows that the EFG's obtained from the self-consistent charge density of the "standard" FLAPW band-structure calculation. As described above, in this "Cu $3p_{\rm core}$" calculation, the Cu $3p$ states are treated fully relativistically as core electrons, i.e., the Cu $3p$ closed shell (and all other core states) is treated as being spherically symmetric and hence can give no contribution to the EFG. The second line of Table I, referred to as "Cu $3p_{\rm val}$," shows the EFG's obtained from the self-consistent charge density when the Cu $3p$ semicore states are relaxed (i.e., treated as band states in a separate window) in the full (nonspherical) potential and thereby allowed to contribute to the EFG at the Cu sites. (These results—which agree with those of Ambrosch-Draxl *et al.*[11]—will be discussed more fully below.) The anisotropy parameters η predicted in both the "Cu $3p_{\rm core}$" and "Cu $3p_{\rm val}$" calculations are in good agreement with the experimentally observed η values;[5,6] the predicted principal axes are also the same as in the experiments, y for Cu(1) and z for Cu(2). However, we find a reversal in the relative ordering [Cu(1) vs Cu(2)] of V_{zz} between the theoretical and experimental values. This result is the same reversal found earlier by us[7] without inclusion of the Sternheimer antishielding corrections (discussed below). Indeed, it was this reversal that was thought to indicate the importance of the Sternheimer corrections and led us to the lengthy calculations reported below. Before we discuss the disagreement and reversal of V_{zz} in detail, let us try to understand the origin of the EFG for Cu(1) and Cu(2) in $YBa_2Cu_3O_7$.

As described in the previous section, the EFG $V_{zz}^{\rm tot}$ can have two contributions: one, $V_{zz}^{\rm MT}$, from the anisotropic charge distribution inside a muffin-tin (MT) sphere and the other, $V_{zz}^{\rm latt}$, from the lattice summation (other muffin-tin regions and interstitials). Thus,

$$V_{zz}^{\rm tot}=V_{zz}^{\rm MT}+V_{zz}^{\rm latt}\ , \tag{13}$$

where the MT contribution $V_{zz}^{\rm MT}$ is given by

$$V_{zz}^{\rm MT}=\left[\frac{4\pi}{2l+1}\right]^{1/2}\int_0^{R_{\rm MT}}\frac{\rho_{zz}(r)}{r^3}r^2dr\ . \tag{14}$$

In Table II, we list the contributions to $V_{zz}^{\rm tot}$ of the muffin-tin part and the lattice part at each Cu(1) and Cu(2) site in the "Cu $3p_{\rm val}$" calculation. We can see that the dominant contributions to V_{zz} for both Cu(1) and Cu(2) arise from $V_{zz}^{\rm MT}$. These results indicate that the most important part of the EFG at the Cu sites in $YBa_2Cu_3O_7$ comes from the anisotropic charge distribution inside the MT spheres (i.e., local charge anisotropy) rather than the external (lattice) charge distribution.

B. FLAPW results for the EFG at other sites

A list of theoretical and experimental values of the EFG at all the atomic sites in $YBa_2Cu_3O_7$ is given in Table III. The overall agreement between the results of the two independent theoretical FLAPW calculations and experiment for the Cu and O sites is seen to be very good. Note particularly the agreement of the principal axes and η values, determined by the theoretical calculations with the observed ones. The principal axes for the EFG at the O sites are in the direction of the Cu—O $dp\sigma$ bonding axis; the EFG anisotropy at the O sites is largely determined by the internal charge anisotropy inside the O MT spheres as will be discussed later and shown in Table

TABLE I. Comparison of the calculated and experimental EFG results at the Cu sites. V_{zz} refers to the largest component and η the anisotropy parameter.

	Cu(1)			Cu(2)		
	V_{zz}	η (10^{22} V m^{-2})	Principal axis	V_{zz}	η (10^{22} V m^{-2})	Principal axis
FLAPW						
Cu $3p_{\rm core}$	0.61	0.66	y	−0.53	0.01	z
Cu $3p_{\rm val}$	0.61	0.79	y	−0.57	0.02	z
Experiment						
[a]	±0.75	0.97	y	±1.23	|0.0±0.24|	z
[b]	±0.74	0.92		±1.23	0.14	

[a]Reference 6.
[b]Reference 5.

TABLE II. Decomposition of V_{zz} for the EFG at Cu(1) and Cu(2) sites obtained by the FLAPW calculations, first into MT and lattice contributions [cf. Eq. (13)] and then into angular components [cf. Eq. (17)]. (V_{zz} in units of 10^{22} V m^{-2}.)

	V_{zz}^{tot}	V_{zz}^{MT}	V_{zz}^{latt}	V_{zz}^{dd}	V_{zz}^{pp}	V_{zz}^{sd}	V_{zz}^{semicore}
Cu(1)	0.613	0.618	−0.005	0.775	−0.166	0.006	0.003
Cu(2)	−0.573	−0.576	0.003	−1.506	0.977	−0.002	−0.046

IV. This is also consistent with the fact that dominant contributions to the EFG at the Cu sites are predominantly from the charge anisotropy inside the MT regions, which arises from the strong anisotropic covalent hybridization of the Cu $d-$O p orbitals. In addition to the agreement of the calculated principal axis and η values with experiment, both theoretical and experimental values of the V_{zz} agree well (the differences between them are within 20%) except for the case of Cu(2) where the calculated V_{zz} is about half of the observed value. The agreement of these results with a similar independent FLAPW calculation by Ambrosch-Draxl *et al.*[11] is very good—except for the EFG results at the Y nucleus which we now discuss.

The differences of the EFG results at the Y sites between these two FLAPW calculations are apparently from the different treatments of the Y 4p states in the two-window calculation. In the calculation of Ambrosch-Draxl *et al.*,[11] the Y 4p semicore states are included in a separate second energy window together with the other Cu 3p, Y 4s, and Ba 5s states but treated as additional band states (i.e., remaining as nonorthogonal to the major valence band states). On the other hand, in our calculation, the Cu 3p, Y 4s, and Ba 5s semicore states are included in a separate energy window with each energy eigenstate being orthogonal to the major valence states which now include the Y 4p states. Now, the energy levels of the Y 4p as well as Ba 5p states are shallow (lying 1.6 and 0.8 Ry below E_F, respectively), and the major energy bands of the Y 5p states lie high ($\approx$1 Ry) above E_F. Since the Y atom is highly ionic, it is difficult to describe the 4p or 5p wave-function character inside the Y MT sphere by taking a separate window for the Y 4p from the Y 5p window. In fact, when we tried to use two windows for the Y 4p and Y 5p states, we had an orthogonality problem with the Y 4p states. Thus, it may be more reasonable to describe the tails of Cu d and O p inside the Y MT spheres by a linearized APW function in the spirit of the LAPW method.[18,19]

TABLE III. Comparison of calculated and experimental EFG results (V_{zz} in 10^{22} V m^{-2}).

		Φ_{xx}	Φ_{yy}	Φ_{zz}	Principal axis	η
Cu(1)	FLAPW[a]	−0.549	0.613	−0.064	y	0.79
	FLAPW[b]	−0.67	0.74	−0.07	y	0.8
	Expt[c]	−0.74	0.75	−0.0	y	0.97
Cu(2)	FLAPW[a]	0.291	0.282	−0.573	z	0.02
	FLAPW[b]	0.30	0.26	−0.56	z	0.1
	Expt[c]	0.62	0.62	−1.23	z	|0.0±0.24|
O(1)	FLAPW[a]	−0.678	1.844	−1.166	y	0.26
	FLAPW[b]	−0.61	1.83	−1.22	y	0.3
	Expt[d]	−0.51	1.73	−1.21	y	0.40
O(2)	FLAPW[a]	1.354	−0.825	−0.529	x	0.22
	FLAPW[b]	1.18	−0.7	−0.48	x	0.2
	Expt[d]	1.05	−0.63	−0.41	x	0.21
O(3)	FLAPW[a]	−0.828	1.375	−0.548	y	0.20
	FLAPW[b]	−0.7	1.19	−0.49	y	0.2
	Expt[d]	−0.63	1.02	−0.39	y	0.24
O(4)	FLAPW[a]	−0.540	−0.733	1.272	z	0.15
	FLAPW[b]	−0.47	−0.7	1.17	z	0.2
	Expt[d]	−0.40	−0.76	1.16	z	0.31
Y	FLAPW[a]	−0.057	0.201	−0.144	y	0.43
	FLAPW[b]	−0.02	−0.32	0.34	z	0.9
Ba	FLAPW[a]	−0.563	−0.060	0.622	z	0.81
	FLAPW[b]	−0.67	−0.06	0.73	z	0.8

[a]Present work.
[b]Reference 11.
[c]Reference 6.
[d]Reference 21.

TABLE IV. Partial charge decomposition of the valence charge density inside MT spheres of each Cu and O atoms in $YBa_2Cu_3O_7$. The contributions from the $3p$ semicore states are given in the parentheses. Also, the values of the MT sphere radius are listed (units in electrons).

	s	p	p_x	p_y	p_z	d	$d_{x^2-y^2}$	d_{xy}	d_{yx}	d_{zx}	d_{z^2}	R_{MT} (a.u.)
Cu(1)	0.2882	0.2649	0.0377	0.0940	0.1332	8.7894	1.6941	1.8692	1.8673	1.8870	1.4718	2.0
		(5.9821)	(1.9943	1.9940	1.9938)							
Cu(2)	0.2482	0.2313	0.0972	0.0899	0.0442	8.8380	1.4766	1.8786	1.8468	1.8447	1.7912	2.0
		(5.9820)	(1.9939	1.9939	1.9942)							
O(1)	1.5841	3.4389	1.2215	0.9432	1.2742							1.6
O(2)	1.5762	3.5193	1.0256	1.2667	1.2271							1.6
O(3)	1.5775	3.5169	1.2688	1.0185	1.2296							1.6
O(4)	1.4902	3.2165	1.1301	1.1490	0.9374							1.49

C. Analysis of the charge density contribution to the EFG

To understand the origin of the nonspherical charge density inside the MT sphere we decompose the nonspherical charge density as following:

$$\rho_{LM}(r)=\sum_{ll'}\rho_{LM}^{ll'}(r)\ , \tag{15}$$

where

$$\rho_{LM}^{ll'}(r)=\sum_{n\mathbf{k}}f(\varepsilon_{n\mathbf{k}})\sum_{mm'}c^{l'm'}{}_{LMlm}R_{lm}^{*}(r,\varepsilon_{n\mathbf{k}})R_{l'm'}(r,\varepsilon_{n\mathbf{k}})\ . \tag{16}$$

Here, $R_{lm}(r,\varepsilon_{n\mathbf{k}})$ represents a radial wave function of the state with angular momentum quantum number lm and energy $\varepsilon_{n\mathbf{k}}$; $c^{l'm'}{}_{LMlm}$, the Clebsch-Gordan coefficients and $f(\varepsilon_{n\mathbf{k}})$, the weighting factor for the $\mathbf{k}$-space integration. For the $L=2$ term of $\rho_{LM}(r)$, only few (ll') contributions remain due to the selection rule in $c^{l'm'}{}_{LMlm}$. The only nonzero contributions to $\rho_{2M}^{ll'}(r)$ are $\rho_{2M}^{pp}(r)$ for $(l=1,\ l'=1)$, $\rho_{2M}^{dd}(r)$ for $(l=2,\ l'=2)$, and $\rho_{2M}^{sd}(r)$ for $(l=0,\ l'=2)$ or $(l=2,\ l'=0)$. Hence we can interpret $\rho_{2M}^{pp}(r)$ as the charge density originating from p wave functions, $\rho_{2M}^{dd}(r)$ from d wave functions, and $\rho_{2M}^{sd}(r)$ from s-d mixtures. By knowing the decomposition of $\rho_{LM}(r)$ we can write down each contribution of $\rho_{2M}^{ll'}$ to the EFG; for example,

$$V_{zz}^{ll'}=\left[\frac{4\pi}{2l+1}\right]^{1/2}\int_0^{R_{MT}}\frac{\rho_{zz}^{ll'}}{r^3}r^2dr\ , \tag{17}$$

where

$$V_{zz}^{MT}=\sum_{ll'}V_{zz}^{ll'}\ . \tag{18}$$

The radial dependence of the nonspherical charge components or Cu(1) and Cu(2) is illustrated in Fig. 1, with the integrand $[\rho_{zz}(r)/r^3]r^2$ for the EFG, i.e., V_{zz}^{MT}, and the integral $V_{zz}^{MT}(R)=\int_0^R[\rho_{zz}(r)/r^3]r^2dr$. As seen in the

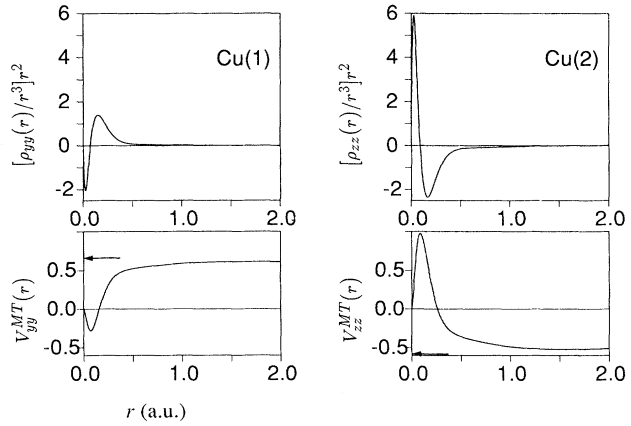

FIG. 1. Radial dependence of the nonspherical charge density components of the integrand of Eq. (17), $[\rho_{yy}(r)/r^3]r^2$ for Cu(1) and $[\rho_{zz}(r)/r^3]r^2$ for Cu(2), and the integral of Eq. (18), $V_{yy}^{MT}(R)$ for Cu(1) and $V_{zz}^{MT}(R)$ for Cu(2). The arrows indicate the total EFG's, V_{zz}^{tot}.

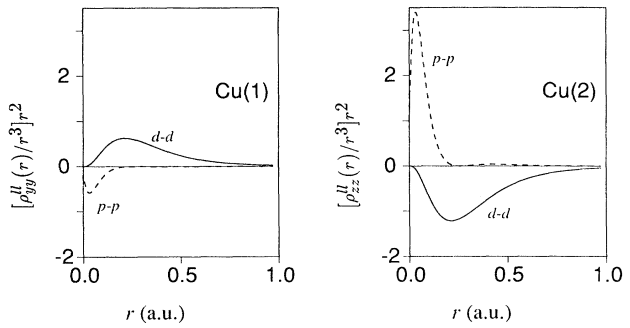

FIG. 2. Partial contributions of ρ^{pp} and ρ^{dd} to the EFG for Cu(1) and Cu(2). Detailed definitions for ρ^{ll}_{zz} and ρ^{ll}_{yy} are given in the text.

figure, the $1/r^3$ factor enhances the contribution of $\rho_{zz}(r)$ near the origin (nucleus) and thus most of the contributions to the EFG arise from the region where $r \leq 1$ a.u.

As shown in Table II, the *s-d* contributions to V_{zz}^{MT} (the so-called "angular excitations"[12,13]) are negligible, while the *p-p* and *d-d* contributions (the so-called "radical excitations"[12,13]) are large. Note that the dominant contributions to V_{zz}^{MT} are from the *d-d* terms, ρ_{zz}^{dd}. From Fig. 2 it is also clear that the *d-d* contributions dominate over the *p-p* contributions. (Since the ρ_{zz}^{sd} contributions to the EFG are so small, only ρ_{zz}^{pp} and ρ_{zz}^{dd} are shown in Fig. 2.) (Note that this result is different from the case of hcp metals studied by Blaha *et al.*[20] where the *p-p* contributions dominate over the *d-d* contributions.) In the cuprate, there are strong anisotropic hybridizations between Cu *d* and O *p* states within the Cu(2) planes and Cu(1) chains. The covalent nature of the Cu *d*–O *p* hybridization leads to the anisotropic radial deformation of the Cu 3*d* wave functions. The resulting anisotropic charge distribution is demonstrated in Table IV, which lists partial charge decompositions inside the Cu(1) and Cu(2) MT spheres. This anisotropic radial deformation gives rise to the huge nonspherical *d-d* charge density shown in Fig. 1. Since there is a large 'intrinsic' quadrupole field provided by the nonspherical (internal) *d-d* charge distribution, the other atomic electrons (*s,p* electrons) are polarized in response to the anisotropic *d-d* charge distributions.

Let us now return to the role of the core electrons on the EFG (Sternheimer antishielding) as determined from the "Cu $3p_{\mathrm{val}}$" calculations. As discussed above, it is clear that the contribution of the internal charge distribution to the EFG is more significant than that of the external (lattice) charge distribution. The Cu 3*d* shell is open and deformed so that there is a strong valence charge contribution to the EFG, denoted as V_{ij}^{v}. Hence, the shielding or antishielding effects due to the closed shell (semi-)core charges are expected to be large. These 3*d* open shell electrons interact with the inner 3*p* shell and give rise to an effective (core polarization) field, V_{ij}^{c},

$$V_{ij}^{c} = -R V_{ij}^{v} , \tag{19}$$

where R represents the Sternheimer (anti-) shielding factor. The R factor for transition metal ions is usually smaller[13] than 0.2.

However, as shown in Table I, the EFG at the Cu sites in $YBa_2Cu_3O_7$ has a very small antishielding contribution from the Cu 3*p* semicore states; the largest contribution to the EFG originates from the anisotropic valence electron charge distribution. Comparing the V_{zz} results with and without the Cu 3*p* "semicore" relaxation (see Table I), we obtain the antishielding factors for Cu(1) and Cu(2) to be

$$R(\mathrm{Cu}(1)) = 0.005 , \tag{20}$$

$$R(\mathrm{Cu}(2)) = 0.08 , \tag{21}$$

which are much smaller than expected. A surprising result is the large difference (a factor of 16) in the R values for Cu(2) and Cu(1).

IV. CHARGE ANISOTROPY VS EFG

The partial charge decomposition listed in Table IV represents a symmetry-decomposed (based upon the symmetrized harmonics) contribution to the total number of electrons inside each MT sphere. We can obtain this number by integrating Eq. (15) over r for $L = M = 0$;

$$n = \int_0^{R_{\mathrm{MT}}} \rho_{00}(r) r^2 dr = \sum_{lm} n_{lm} , \tag{22}$$

where

$$n_{lm} = \int_0^{R_{\mathrm{MT}}} \rho_{00}^{lm}(r) r^2 dr = \sum_{n_{\mathbf{k}}} f(\varepsilon_{n\mathbf{k}}) \int_0^{R_{\mathrm{MT}}} R_{lm}^{*}(r;\varepsilon_{\mathbf{k}}) R_{lm}(r;\varepsilon_{\mathbf{k}}) r^2 dr . \tag{23}$$

Since the integration for n_{lm} is done up to $r = R_{\mathrm{MT}}$, the electron number n_{lm} depends on the choice of the MT sphere radius. Although the n_{lm} values have no absolute meaning, some information can be obtained by comparing their relative values.

From Table IV it is clear that the anisotropy of the charge distribution is due to the covalent nature of the Cu *d*–O *p* hybridization. As discussed in our earlier band-structure results for $YBa_2Cu_3O_7$,[2] there are four bands—each consisting of Cu(2) *d*–O(2) *p*–O(3) *p* orbitals and Cu(1) *d*–O(1) *p*–O(4) *p* orbitals—that cross E_F. Two strongly dispersed bands consist of Cu(2) $d_{x^2-y^2}$–O(2) p_x–O(3) p_y combinations and are about half-filled; the Cu(1) $d_{z^2-y^2}$–O(1) p_x-O(4) p_z antibonding band is almost entirely unoccupied; the $dp\pi$ antibonding band of Cu(1) d_{yz}–O(1) p_z–O(4) p_y orbitals is almost entirely occupied. As demonstrated in Table IV, due to the strong hybridization of Cu-O $dp\sigma$ orbitals, the number of electrons in the Cu and O orbitals forming the $dp\sigma$ states is much smaller than the others. Thus, the occupation number for the Cu(2) $d_{x^2-y^2}$ state is much smaller than that of the Cu(2) d_{xy}, d_{yz}, d_{z^2} states. Similarly, the O(2) p_x and O(3) p_y states have a much smaller occupation that do the other O(2) $p_{y,z}$ and O(3) $p_{z,x}$ states.

In addition to the anisotropy in the 3*d* electron charge distribution of Cu, the anisotropy of the Cu 4*p* partial

valence charge distribution is also significant. Although the number of occupied Cu $4p$ components is small, their anisotropy (i.e., directional dependence) is very large because the origin of their occupation arises from the tails of neighboring O p wave functions. Hence, the anisotropy character of each $4p$ component (i.e., p_x, p_y, and p_z) at Cu(1) and Cu(2) is well correlated with the distance to the near neighbor oxygen in each direction.

Now, let us look in detail into the relation between the charge anisotropy and the EFG. For the case of Cu(2), the η value is nearly equal to zero. That is, the Φ_{2m} components in Eq. (11) are nearly zero for $m \neq 0$; alternatively, the $\Phi_{2M} = \sqrt{4\pi/5} \int (\rho_2 M r^3/r^2) dr$ is nearly zero for $M \neq 0$. Hence, Φ_{20} and ρ_{20} can be the only major parameters in determining the EFG for Cu(2). (Note that $\Phi_{20} \propto V_{zz}$.) From Eqs. (16) and (17) we can define a charge anisotropy number[20]

$$\Delta n_{zz} = \Delta n_p + \Delta n_d \tag{24}$$

with

$$\Delta n_p = \tfrac{1}{2}(n_{p_x} + n_{p_y}) - n_{p_z} , \tag{25}$$

$$\Delta n_d = (n_{d_{x^2-y^2}} + n_{d_{xy}}) - \tfrac{1}{2}(n_{d_{yz}} + n_{d_{zx}}) - n_{d_{z^2}} . \tag{26}$$

This decomposition of charge anisotropy is to be compared with the decomposition of the nonspherical charge contribution to the EFG, as shown in Eq. (18) and Table II. In order to show the relation between the charge anisotropy Δn_l and its contribution to the EFG V_{zz}^{ll}, the charge anisotropy number Δn_l for each l component and its contribution to V_{zz}^{ll} are listed in Table V, together with the ratio $\chi_l = V_{zz}^{ll}/\Delta n_l$, which represents an effective quadrupole $\langle\langle 1/r^3 \rangle\rangle_l$ value per each partial valence electron charge. That is,

$$\chi_l = \frac{V_{zz}^{ll}}{\Delta n_l} = \left[\frac{4\pi}{2l+1}\right]^{1/2} \frac{\int_0^{R_{\rm MT}} \frac{\rho_{zz}^{ll}}{r^3} r^2 dr}{\int_0^{R_{\rm MT}} \rho_{zz}^{ll} r^2 dr} = \left\langle\!\!\left\langle \frac{1}{r^3} \right\rangle\!\!\right\rangle_l . \tag{27}$$

As seen in Table V, the χ_l demonstrate the sensitivity of each partial charge component to the EFG. For example, if one assumes that there is one hole localized at the Cu(2) site with $d_{x^2-y^2}$ symmetry (this is often the case of several model Hamiltonians taken in high-T_c theories), then the EFG V_{zz} (in V m^{-2}) is determined by

$$V_{zz} = \left\langle\!\!\left\langle \frac{1}{r^3} \right\rangle\!\!\right\rangle_d \Delta n_d = 5.3 \times 10^{22} \tag{28}$$

with $\Delta n_d = 1$ and $\langle\langle 1/r^3 \rangle\rangle_d = 5.3 \times 10^{22}$ V m^{-2}. However, this value of EFG for Cu(2) is about five times larger than that experimentally observed, which makes it difficult to believe that there is a localized hole with a definite symmetry like $d_{x^2-y^2}$ at the Cu(2) site.

With these results before us, let us now return to the earlier mentioned disagreement of the FLAPW results with experiment. It is, at first sight, surprising that even a highly precise FLAPW calculation gives an EFG value for Cu(2) which is about half of the observed value. Examination of the results shows, however, that this is a very delicate problem because assuming a very small change of the anisotropic charge distribution can produce perfect agreement with experiment. For example, as suggested by Ambrosch-Draxl *et al.*,[11] a charge transfer of 0.06 electrons from the $d_{x^2-y^2}$ state to the d_{z^2} state can reproduce experiment. We find an even more remarkable result: a transfer of only 0.0014 electrons from the $3p_x$ and $3p_y$ states to the $3p_z$ state can produce the same result, namely, perfect agreement with experiment. Such a small transfer is easily achievable even in semicore states like the $3p$ in Cu.

TABLE V. Charge anisotropy count Δn_l, its corresponding EFG contribution and the ratio $\chi_l = \Delta V_{zz}^{ll}/\Delta n_l$ for Cu(2).

	p	d	$3p$ semicore
Δn_l	0.049	−0.282	−0.0003
ΔV_{zz}^{ll}	0.977	−1.506	−0.046
χ_l	20.	5.3	15.3

V. CONCLUDING REMARKS

We found that the main contribution to the EFG at the Cu sites in $YBa_2Cu_3O_7$ comes from the intrinsic quadrupole field provided by the nonspherical (internal) charge distribution which is due to the covalent nature of the Cu d–O p hybridization. Similarly, the EFG anisotropy at the O sites is also largely determined by the internal charge anisotropy inside the O atoms, where the principal axes for the EFG at the O sites are in the direction of the Cu–O $dp\sigma$ bonding axis. As shown in Table III,[21] the agreement between the theoretical FLAPW results and experiment for the principal axis and η values at the Cu and O sites are excellent. Further, both theoretical and experimental V_{zz} values agree well except for the case of Cu(2). The difference in the V_{zz} values at Cu(2) between theory and experiment may arise from the theoretical mistreatment of the semicore $3p$ states of Cu since the resulting V_{zz} is highly sensitive to the anisotropy of the $3p$ occupation.

This sensitivity of the EFG results to $3p$ occupation highlights the importance of these semicore states as well as their proper theoretical treatment. Thus, it is important to emphasize that there are still problems left in the theoretical description of the Cu $3p$ semicore states. Now, even though we have carried out "two-window" calculations to treat the Cu $3p$ state separately from the valence $4p$ state, problems still remain arising when the $3p$ semicore states are included as band states. First, treating localized $3p$ semicore electrons as band states is a somewhat unnatural description; it is done in order to allow them to assume a nonspherical distribution and hence to obtain an angular dependent potential (arising from the $3p$ semicore states) at the nuclear site. In prac-

tice, this treatment increases considerably the numerical difficulties of the calculation because the APW basis and the corresponding expansion of the potential (as well as charge density) must be enlarged considerably in order to obtain a proper description of these rather localized semicore states. Second, in the FLAPW method, the wave functions in the band state are calculated in a semirelativistic way, the ones in the core states are treated fully relativistically. In fact, when they are treated as core electrons, the Cu $3p$ semicore levels lie at -71.65 eV ($j=\frac{1}{2}$) and -69.03 eV ($j=\frac{3}{2}$) below E_F for Cu(1) and at -71.48 eV ($j=\frac{1}{2}$) and -68.86 eV ($j=\frac{3}{2}$) below E_F for Cu(2). For both cases, the spin-orbit coupling gives an energy difference $\Delta E=2.62$ eV between the $j=\frac{1}{2}$ and $\frac{3}{2}$ states. However, when we treat the $3p$ semicore states as semirelativistic band states, these spin-orbit effects are totally neglected. These approximations, made to the $3p$ semicore states in the band states, can have a large impact on the EFG result due to their high sensitivity to the EFG at the Cu sites.

All these results emphasize that the EFG is an extremely sensitive quantity that requires highly reliable accuracy in its calculation. It is thus quite remarkable that the FLAPW band calculations based upon density functional theory with the LDA approximation can provide a reasonable description for understanding the electronic structure and EFG values in high-T_c $YBa_2Cu_3O_7$ compounds.

ACKNOWLEDGMENTS

Work at Northwestern University was supported by the National Science Foundation (through the Northwestern University Materials Research Center, Grant No. DMR88-21571 and by a computing grant from its Division of Advanced Scientific Computing at the Pittsburgh Supercomputing Center) and the Office of Naval Research (Grant No. N00014-89-J-1290). Work at the University of Vienna was supported by the Austrian "Fonds zur Förderung der wissenschaftlichen Forschung" by projects Nr. 6835-PHY and 7064-PHY.

APPENDIX A: TWO-WINDOW FLAPW CALCULATIONS

In a standard FLAPW band-calculation method, a single set of energy parameters is usually taken for the expansion of the LAPW (linearized-augmented-plane-wave) basis functions. In the LAPW method,[18,19] it is necessary to choose the values of the energy parameters to lie at the center of the occupied bands, weighted according to the angular decomposition inside the MT spheres, in order to have an optimal description of the radial functions for the LAPW basis. However, there is a problem of including two valence band states with the same l character but in different energy shells, like $3p$ and $4p$ states of Cu or $5p$ and $6p$ states of Cs. In such cases, it is natural to introduce two sets of energy parameters for the proper description of the radial wave functions within each energy range (i.e., energy window). This means that there is a set of the LAPW basis functions $\{\phi_j^W\}$ for the corresponding set of energy parameters $\{E_l^W\}$:[18,19]

$$\phi_j^W(\mathbf{k})=\phi^W(\mathbf{K}_j)=\begin{cases}\Omega^{-1/2}\exp(i\mathbf{K}_j\cdot\mathbf{r}) & \text{in the interstitial region,}\\ \sum_{lm}[a_{lm}^{\alpha W}(\mathbf{K}_j)u_l^{\alpha W}(r)+b_{lm}^{\alpha W}(\mathbf{K}_j)\dot{u}_l^{\alpha W}(r)]Y_{lm}(\hat{r}) & \text{inside the } \alpha\text{th MT sphere,}\end{cases} \tag{A1}$$

with $\mathbf{K}_j=\mathbf{k}+\mathbf{G}_j$, where W represents a number for each energy window, $\mathbf{k}$ is a reduced vector inside the first BZ, and $\mathbf{G}_j$ is a reciprocal lattice vector. The functions $u_l^{\alpha W}(r)\equiv u_l^{\alpha}(E_l^W;r)$ and $\dot{u}_l^{\alpha W}(r)\equiv\dot{u}_l^{\alpha}(E_l^W;r)$ are the radial solutions to the semirelativistic Dirac equation and the energy derivative of the radial solutions with energy parameter E_l^W for an energy window W inside the αth MT sphere. The coefficients $a_{lm}^{\alpha W}(\mathbf{K}_j)$ and $b_{lm}^{\alpha W}(\mathbf{K}_j)$ are determined by matching the required boundary conditions at the MT-sphere boundary. From now on, for simplicity in the representation, we will write the LAPW basis function for the energy window W as

$$\phi_j^W=\begin{cases}\Omega^{-1/2}\exp(i\mathbf{K}_j\cdot\mathbf{r}) & \text{in the interstitial region,}\\ \sum_{lm}a_{lm}^{\alpha W}(\mathbf{K}_j)u_l^{\alpha W}(r)Y_{lm} & \text{inside the } \alpha\text{th MT sphere,}\end{cases} \tag{A2}$$

with the reduced vector $\mathbf{k}$.

Now, for each energy window W, we can set up a variational equation for a trial solution $\varphi_{\mu\mathbf{k}}^W=\sum_j z_{j\mu}^W\phi_j^W$ with a Hamiltonian H_0, which includes the full potential in the interstitial region but neglects all nonspherical terms inside the MT spheres. This is called a "first-variational" calculation. By solving the matrix equation

$$\sum_j H_{0ij}^W z_{j\mu}^W=\varepsilon_\mu^W\sum_j S_{ij}^W z_{j\mu}^W\ , \tag{A3}$$

where

$$H_{0ij}^W=\langle\phi_i^W|H_0|\phi_j^W\rangle,\quad S_{ij}^W=\langle\phi_i^W|\phi_j^W\rangle\ ,$$

we obtain the eigenvalues and corresponding eigenvectors:

$$\varphi^W_{\mu\mathbf{k}}=\sum_j z^W_{j\mu}\phi^W_j = \begin{cases}\sum_j z^{\mu W}_j \Omega^{-1/2}\exp(i\mathbf{K}_j\cdot\mathbf{r}), \\ \sum_{lm} A^{\alpha W}_{lm}(\mu\mathbf{k})u^{\alpha W}_l(r)Y_{lm},\end{cases} \tag{A4}$$

where

$$A^{\alpha W}_{lm}(\mu\mathbf{k})=\sum_j z^W_{j\mu}a^{\alpha W}_{lm}(\mathbf{K}_j)\ .$$

The set of (energy) eigenfunctions $\{\varphi^W_{\mu\mathbf{k}}\}$ for all energy windows, which are obtained as a result of the first variational calculation, is used as a basis set for a "second-variational" calculation which includes the nonspherical potential terms inside MT spheres which were left out in the first-variational calculation. Since, however, the electronic states for each energy window are treated and diagonalized separately in the first-variational calculation, there exists a small nonorthogonality between wave functions of different energy windows. Generally, this overlap is very small and can be neglected. But, in some calculations, the extended degree of freedom for the valence states which lie close together (e.g., Ba $5p$ and $6p$ states) can lead to an overcompleteness problem. An inclusion of the nonorthogonality in the second-variation calculation is also important for the highly sensitive EFG calculations.[14]

In the second variation, the basis of the Hamiltonian matrix will cover the multiwindow space of $\{\varphi^W_{\mu\mathbf{k}}|W=1,2,\ldots\}$. Since the basis set of the multiwindow wave functions $\{\varphi^W_{\mu\mathbf{k}}|W=1,2,\ldots\}$ are not orthogonal among wave functions of different windows, the overlap matrix

$$\langle\varphi^W_{\mu\mathbf{k}}|\varphi^{W'}_{\mu'\mathbf{k}}\rangle=S^{WW'}_{\mu\mu'}(\mathbf{k}) \tag{A5}$$

appears instead of

$$\langle\varphi^W_{\mu\mathbf{k}}|\varphi^{W'}_{\mu'\mathbf{k}}\rangle=\delta_{\mu\mu'}\delta_{WW'}\ . \tag{A6}$$

Hence, the matrix elements and equations are rewritten by

$$\langle\varphi^W_{\mu\mathbf{k}}|H_0|\varphi^{W'}_{\mu'\mathbf{k}}\rangle=\tfrac{1}{2}[\varepsilon^W_\mu(\mathbf{k})+\varepsilon^{W'}_{\mu'}(\mathbf{k})]S^{WW'}_{\mu\mu'}(\mathbf{k}) =H^{WW'}_{0_{\mu\mu'}}\ , \tag{A7}$$

$$\langle\varphi^W_{\mu\mathbf{k}}|H_{NS}|\varphi^{W'}_{\mu'\mathbf{K}}\rangle=H^{WW'}_{NS_{\mu\mu'}}\ , \tag{A8}$$

and

$$\sum_{\mu'W'}(H^{WW'}_{0_{\mu\mu'}}+H^{WW'}_{NS_{\mu\mu'}})\bar{z}^{W'}_{\mu'n}=\bar{\varepsilon}_n\sum_{\mu'W'}S^{WW'}_{\mu\mu'}\bar{z}^{W'}_{\mu'n}\ . \tag{A9}$$

Solving the matrix equation we finally obtain the eigenvalues and corresponding eigenvectors for the full Hamiltonian:

$$\psi_{n\mathbf{k}}=\sum_{\mu W}\bar{z}^W_{\mu n}\varphi^W_{\mu\mathbf{k}} = \begin{cases}\sum_j \bar{z}_{jn}\Omega^{-1/2}\exp(i\mathbf{K}_j\cdot\mathbf{r}) \\ \sum_{lmW}\tilde{A}^{\alpha W}_{lm}(n\mathbf{k})u^{\alpha W}_l(r)Y_{lm},\end{cases} \tag{A10}$$

where

$$\bar{z}_{jn}=\sum_{\mu W}z^W_{j\mu}\bar{z}^W_{\mu n},\quad \tilde{A}^{\alpha W}_{lm}=\sum_\mu A^{\alpha W}_{lm}(\mu\mathbf{k})\bar{z}^W_{\mu n}\ .$$

[1]S. Massidda, J. Yu, A. J. Freeman, and D. D. Koelling, Phys. Lett. A **122**, 198 (1987).

[2]J. Yu, S. Massidda, A. J. Freeman, and D. D. Koelling, Phys. Lett. A **122**, 203 (1987).

[3]W. W. Warren Jr., R. E. Walstedt, G. F. Brennert, G. P. Espinosa, and J. P. Remeika, Phys. Rev. Lett. **59**, 1860 (1987).

[4]I. Furo, A. Jánossy, L. Mihály, P. Bánkie, I. Pócsik, I. Bakonyi, I. Heinmaa, E. Joon, and E. Lippmaa, Phys. Rev. B **36**, 5690 (1987).

[5]M. Mali, D. Brinkmann, L. Pauli, J. Roos, H. Zimmermann, and J. Hulliger, Phys. Lett. A **124**, 112 (1987).

[6]C. H. Pennington, D. J. Durand, D. B. Zax, C. P. Slichter, J. P. Rice, and D. M. Ginsberg, Phys. Rev. B **37**, 7944 (1988).

[7](Unpublished).

[8]H. J. F. Jansen and A. J. Freeman, Phys. Rev. B **30**, 561 (1983).

[9]P. Blaha, K. Schwarz, and P. Herzig, Phys. Rev. Lett. **54**, 1192 (1985).

[10]P. Blaha and K. Schwarz, J. Phys. F **17**, 899 (1987).

[11]C. Ambrosch-Draxl, P. Blaha, and K. Schwarz, J. Phys. Condens. Matter **1**, 4491 (1989); Physica C **162-164**, 1353 (1989).

[12]R. M. Sternheimer, Phys. Rev. **95**, 736 (1954).

[13]A. J. Freeman and R. E. Watson, Phys. Rev. **131**, 2566 (1963).

[14]We thank P. Blaha and K. H. Schwarz for helpful discussions about the importance of two windows in the FLAPW calculations. In our case we take into account the nonorthogonality between semicore and valence electrons by using the second variation method.

[15]P. Herzig, Theor. Chim. Acta (Berlin) **67**, 323 (1985).

[16]M. Weinert, J. Math. Phys. **22**, 2433 (1981).

[17]M. A. Beno, L. Soderholm, D. W. Capone II, D. G. Hinks, J. D. Jorgensen, I. K. Schuller, C. U. Segré, K. Zhang, and J. D. Grace, Appl. Phys. Lett. **51**, 57 (1987).

[18]D. D. Koelling and G. O. Arbman, J. Phys. F Metal Phys. **5**, 2041 (1975).

[19]O. K. Andersen, Phys. Rev. B **12**, 3060 (1975).

[20]P. Blaha, K. Schwarz, and P. H. Dederichs, Phys. Rev. B **37**, 2792 (1988).

[21]M. Horvatić, Y. Berthier, P. Butaud, Y. Kitaoka, P. Ségransan, C. Berthier, H. Katayama-Yoshida, Y. Okabe, and T. Takahashi, Physica C **159**, 689 (1989).